

Failure Analysis of AISI 304 Stainless Steel Sleeve Used in High-Pressure Hose Assembly of Actuation System of a Satellite Launch Vehicle

V. Murugesan · P. S. Sreejith · Sushant K. Manwatkar ·
S. Sankar Narayan · S. V. S. Narayana Murty · P. Ramesh Narayanan

Submitted: 7 September 2016/in revised form: 30 November 2016/Published online: 10 January 2017
© ASM International 2017

Abstract Hydraulic control actuation systems in launch vehicles use flexible hoses for transmission of forces to actuators at different locations. The hose ends are connected to the interface adapters by AISI 304 stainless steel sleeves. These sleeves are assembled to nipple end fittings of the high-pressure hose by a swaging operation to obtain leak-proof hose assemblies. The swaging operation is carried out at room temperature by a hydraulically operated swaging machine. Performance of the system as a whole requires strict adherence to the quality standards maintaining the critical interface dimensions within specified tolerances and ensuring the compression given to the swaged joint through the sleeve. If the joining forces are less, this can result in loose joints and gross leakage, whereas excessive compression can cause damage to the parts of the system namely the sleeve, stainless steel braid, PTFE or the adapter. The swaged joint is a single-point failure mode, indicating that a failure in the joint can lead to mission failure. It has to withstand harsh environments such as high pressure, low and high temperature extremes, fatigue loading due to pressure cycling as well as vibration. Therefore, as part of design verification, a detailed qualification plan has been prepared and the hoses were tested as per the plan. As per the test plan, these hoses undergo acceptance tests which include pneumatic and hydraulic pressure testing. During acceptance testing of hoses, one of

the hose sleeves was found to be cracked. The cracking was observed after carrying out the pneumatic test when the assembly was being prepared for hydraulic pressure set-up. This paper describes the detailed metallurgical investigation carried out to understand the cause of failure and actions taken to avoid similar failures.

Keywords Flexible hose · AISI 304 sleeve · Swaging · Cracking · Sensitization · Inclusions

Introduction

Hydraulic control actuation systems are used in aircrafts and launch vehicles due to the advantages in terms of their capability to transmit the forces to actuators at different locations through appropriate plumbing, higher torque to mass ratio and ease of installation. Considering these advantages, control surfaces of Reusable Launch Vehicle (RLV) on the winged body technology demonstrator vehicle (TDV) and first-stage solid rocket of a Reusable launch vehicle were actuated by a single hydraulic power source located at the fore end of the TDV.

Depending on the system requirements, the hydraulic plumbing is made in different segments connecting the subsystems like the pump, reservoir, accumulator, manifolds, valves, regulators. This is comprised of both rigid plumbing and flexible hoses. Flexible hoses are necessary to make connections between different subsystems located within a complex sub-assembly, where relative motions are involved and where high vibrations are expected. PTFE hose with stainless steel braid as reinforcement has been selected as the flexible hose for the present application. The interface of the hose with the end adapter is given in Fig. 1. The failure of basic hose, the swaged joint with adapter or

V. Murugesan · S. K. Manwatkar · S. Sankar Narayan ·
S. V. S. Narayana Murty (✉) · P. Ramesh Narayanan
Vikram Sarabhai Space Centre, Thiruvananthapuram 695022,
India
e-mail: susarla.murty@gmail.com

P. S. Sreejith
Cochin University College of Engineering, Kuttanad 688504,
India

Fig. 1 Schematic showing the swaged joint interface of hose assembly

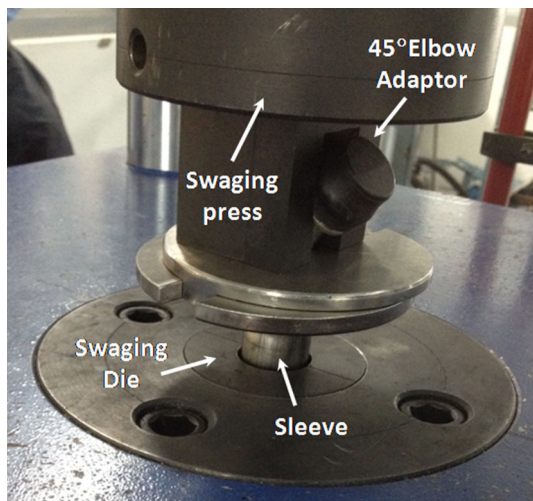
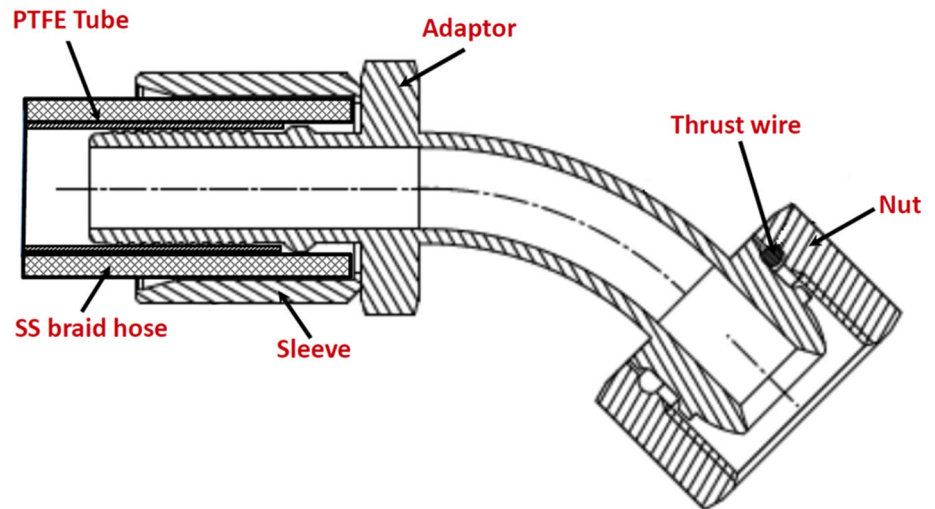


Fig. 2 Digital photograph showing the swaging process

the metal–metal sealing bull nose adapter joints are single-point failure modes for the hose as well as the control system. Performance of the system as a whole requires strict adherence to the standards meeting critical interface dimensions within specified tolerances and controlled compression given to the swaged joint through the sleeve.

To avoid failures in the swaged joint, it is important to control key parameters that affect the gripping force of the joint. Towards this, all aspects related to the alignment of the hose with respect to swaging die, end preparations of the hose and the process parameters of the swaging machine were addressed and finalized. The swaging operation was carried out at room temperature using hydraulically operated swaging machine (Fig. 2). These hoses are swaged with the end adapters with a metal-to-metal sealing interface for making further connections. The swaging operation is carried out by pushing the swage



Fig. 3 Digital photograph showing the cracking of sleeve in hydraulic pressure set-up (a) and after removal from the set-up (b)

assembly with the AISI 304 stainless steel sleeve through a fixed swaging die. The outer diameter of the sleeve gets reduced from one end to the other, and in the process develops a compressive force which grips the hose against the serrations provided in the adaptor, making a permanent joint.

Considering wide variations that can result during the manufacturing of the hose, adapter, swaging process and overall system integrity, a detailed design/process verification plan was made in terms of qualification and

acceptance test procedures. The qualification tests include leak checks with pneumatic pressure testing up to 10 bar, hydraulic pressure testing at working pressure (220 bar) and proof pressure (330 bar), low and high temperature tests followed by proof pressure tests, impulse pressure test and burst test (440 bar) followed by system-level vibration test. With the design and process controls that were implemented, no failure was expected during qualification testing. However, during qualification testing of hoses, one

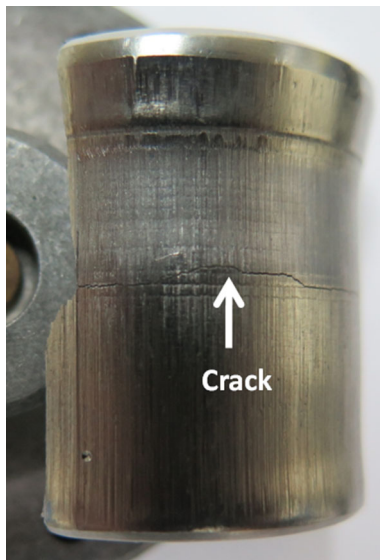


Fig. 4 Photograph showing the circumferential crack on the sleeve

of the AISI 304 hose sleeves was found to be cracked as shown in Fig. 3a. The cracking was observed after carrying out the pneumatic test (at 10 bar pressure for 5 min) when the assembly was being prepared for hydraulic pressure set-up. The hose was removed from the hydraulic pressure set-up and kept aside. The crack was found to grow after the removal from the test set-up and was found to be completely opened up after some time (~ 2 h) as shown in Fig. 3b. Detailed metallurgical analysis was carried out on the cracked sleeve to find out the reasons for cracking. This paper describes the details of the failure that occurred in the swaged joint during the process of qualification of the hoses, identification of root cause and actions taken to avoid similar failures.

Experimental

The cracked sleeve was examined visually, and observations were recorded using digital camera. The fracture surface, surface of the sleeves and metallographically prepared specimens were examined under Carl Zeiss EVO-50 scanning electron microscope (SEM). The chemical composition of the micro-constituents was obtained using Oxford-INCA Energy dispersive X-ray spectroscope (EDS) attached to the SEM. The sleeve was sectioned longitudinally and was metallographically polished with a series of silicon carbide papers, and final polishing was conducted with alumina suspension and one micron diamond lapping compound. The specimens were etched with acetic

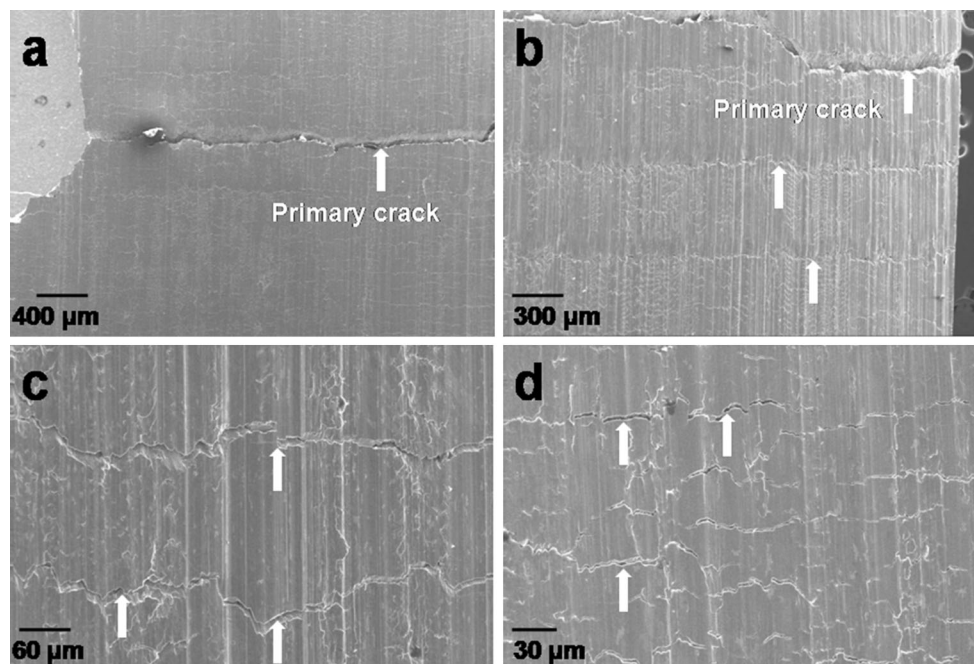


Fig. 5 SEM images showing the circumferential micro-cracks near to the primary crack

glyceregia reagent (HCl—15 ml, HNO₃—10 ml, acetic acid—10 ml and glycerol—5 ml) to reveal the microstructural features. Microstructural observations were made using an Olympus GX-71 optical microscope, and microphotographs were recorded. Microhardness measurements were carried using Wilson Tukon Microhardness tester using a Vickers indenter at 100gf load.

Results

Visual observations of the cracked sleeve revealed a rough surface with die mark lines along the length of the sleeve (Fig. 4). The primary crack was initiated from the outside



Fig. 6 SEM image showing a full view of the fracture surface through the complete thickness of the sleeve

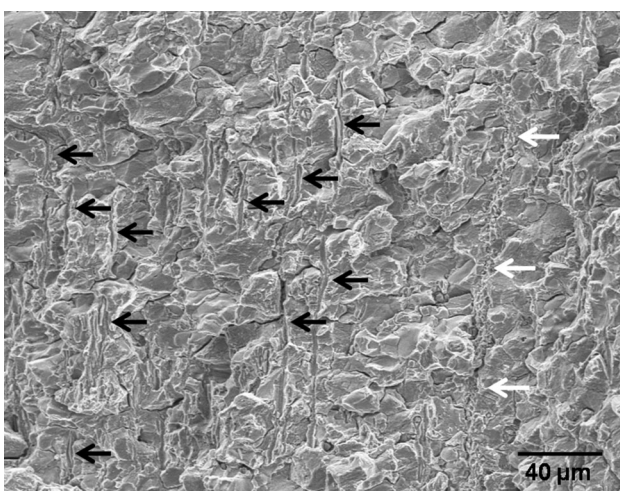


Fig. 7 SEM image showing an isolated large-size silicate inclusion (indicated by white arrows) and uniformly distributed sulphide inclusion stringers (indicated by black arrows) at the location of crack path deviation

diameter (OD) of the tubular sleeve. The primary crack was circumferential and deviated along the length during propagation causing complete separation of the longitudinal crack (Figs. 3 and 4).

SEM observations on the surface of the sleeve near to the crack location revealed circumferential micro-cracks near to the primary crack as shown in Fig. 5. Figure 5a shows the primary crack (indicated by arrow). Figure 5b shows the primary crack at the top of the image and two micro-cracks below the primary crack. Figure 5c shows a higher magnification view of the two micro-cracks shown in Fig. 5b. Figure 5d shows a micrograph of numerous fine micro-cracks on the surface.

The fracture surface of the deviated crack which has opened up and separated into two parts was observed under SEM. Figure 6 shows the full view of fracture surface covering the complete thickness of the sleeve. It also shows the location of the crack path deviation from a circumferential crack to the longitudinal crack. At the location of crack path deviation, a large-size silicate inclusion stringer and uniformly distributed sulphide stringers were observed (Fig. 7). The high-magnification view of the large-size silicate stringer and sulphide stringers is shown in Figs. 8 and 9, respectively. The fracture surface had shown a predominantly intergranular mode of failure (Fig. 10).

Metallographically prepared specimens were observed under optical microscope for inclusion content. The observations revealed the presence of uniformly distributed sulphide inclusions and oxide inclusions in the material as shown in Fig. 11a. Isolated long silicate inclusion stringers were also present in the material (Fig. 11b–d). Very long silicate inclusion stringers of size 2.2 and 1.16 mm size were also observed in the microstructure and are shown in Fig. 12a and b, respectively.

Microstructural observations at the crack location revealed that the crack originated from the outer diameter (OD) of the sleeve and propagated inwards. Two micro-cracks of 250 and 400 μm size originating from OD were also observed near to the primary crack as shown in Fig. 13a. Small deviations of the primary crack were noticed at the intersection of the crack path with a silicate inclusion stringer (Fig. 13a and b). Very fine micro-cracks of 20–30 μm were noticed at the outer edge of sleeve at higher magnification. Deformed and elongated grains were noticed at the OD edge up to approximately 400 μm from the surface. Equiaxed grains were observed at the interior of the sleeve (Fig. 14). Cracking was completely along the grain boundaries throughout the crack path as shown in Fig. 15a. The grain boundaries were decorated with chromium carbide particles (Fig. 15). Microhardness measurements indicated hardness of 470HV_{100gf} at outer edge and 340HV_{100gf} at the middle of the sleeve.

Fig. 8 High-magnification SEM images showing an isolated large-size silicate inclusion on the fracture surface

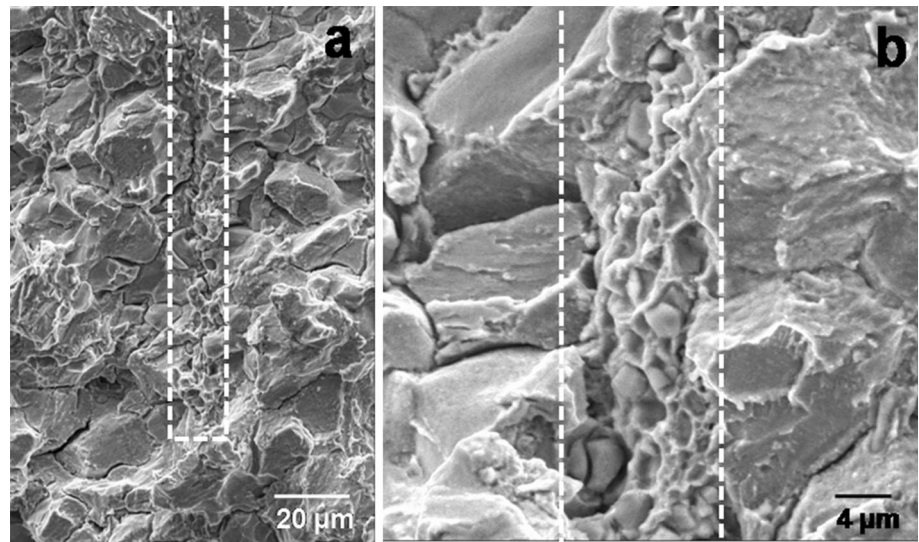


Fig. 9 High-magnification SEM images showing sulphide inclusion stringers on the fracture surface

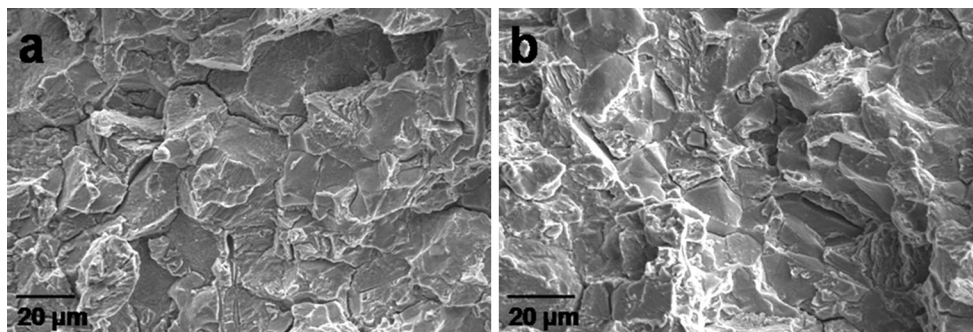
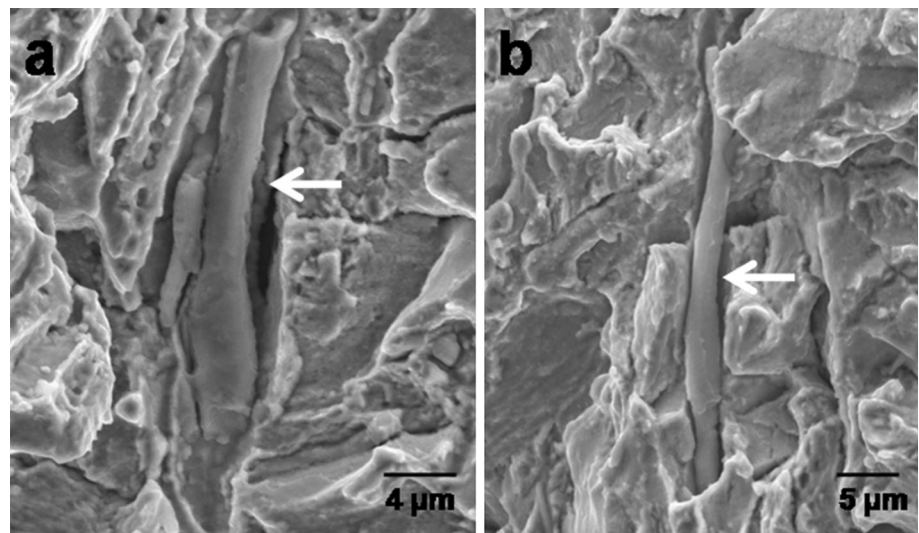


Fig. 10 SEM images on the fracture surface showing the intergranular mode of cracking

EDS analysis on the silicate inclusion stringers revealed the presence of calcium silicates along with manganese sulphide (Fig. 16). The sulphide inclusions were confirmed

to be MnS composition as shown in Fig. 17. The precipitates at grain boundaries were confirmed to be chromium carbide precipitates (Fig. 18).

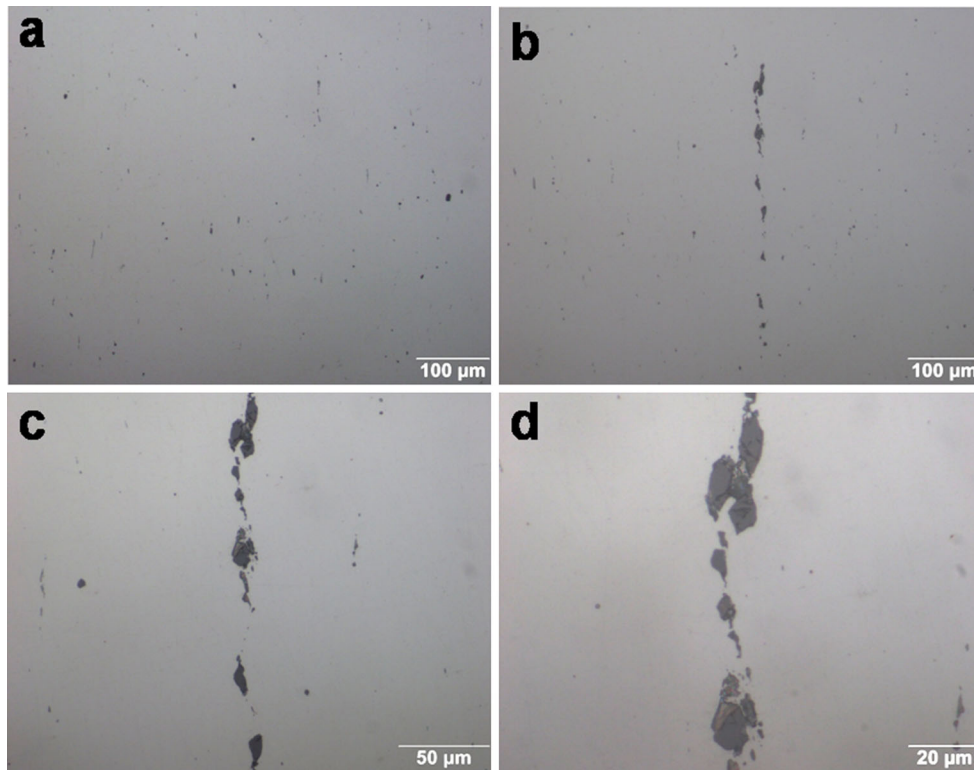


Fig. 11 Optical micrographs in the unetched condition showing (a) sulphide and oxide inclusions, (b) silicate inclusion stringer, (c, d) silicate inclusion stringers at high magnification

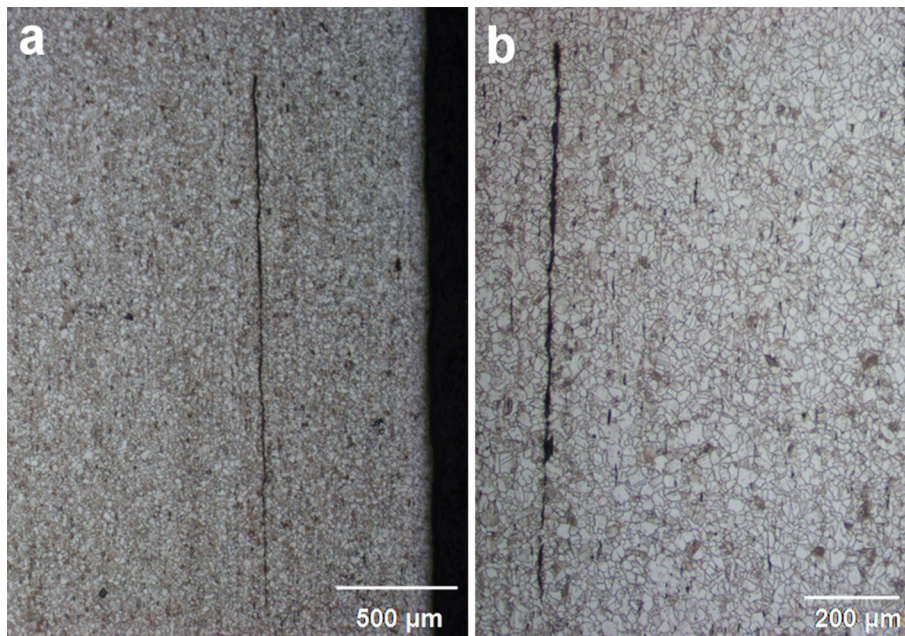


Fig. 12 Optical micrographs showing very long silicate inclusions

Discussion

The microstructural observations revealed that the primary circumferential crack has initiated from the OD of the

sleeve and propagated inwards. The longitudinal die marks observed on the surface of the sleeve along with numerous micro-cracks observed near the primary crack (as indicated by SEM observations shown in Fig. 5) and optical

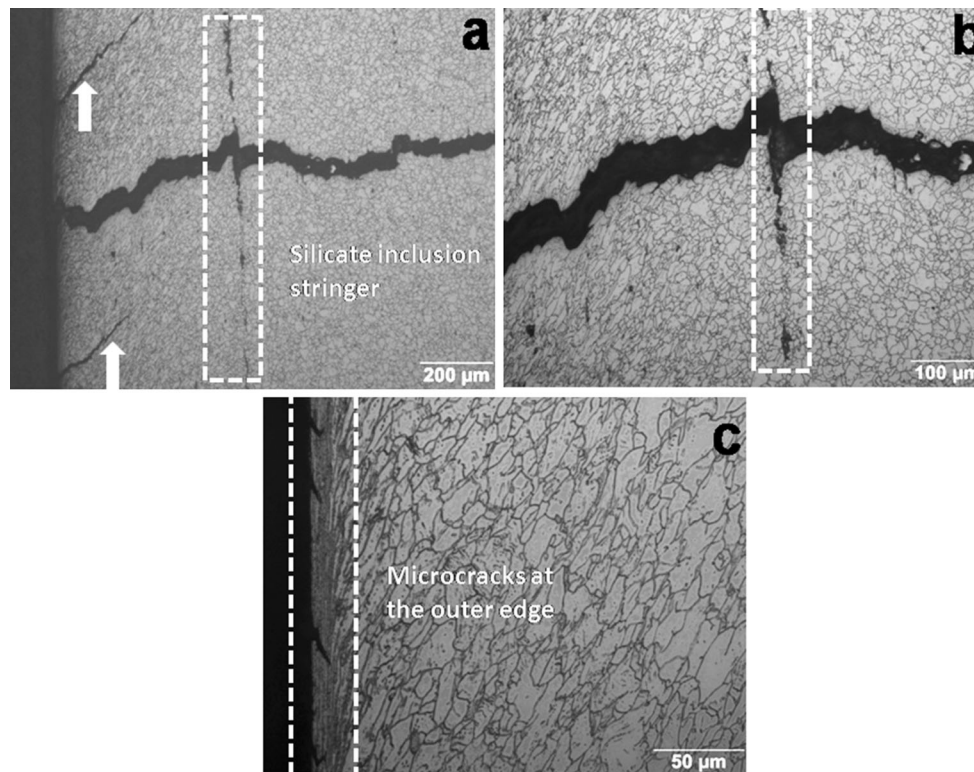


Fig. 13 Optical micrographs showing (a) two micro-cracks of size 250 and 400 μm indicated by arrows near to the primary crack and silicate inclusion stringer along the crack path, (b) little deviation of the crack at the intersection with silicate inclusion stringer, (c) numerous small size micro-cracks of size 20–30 μm at outer edge of the sleeve

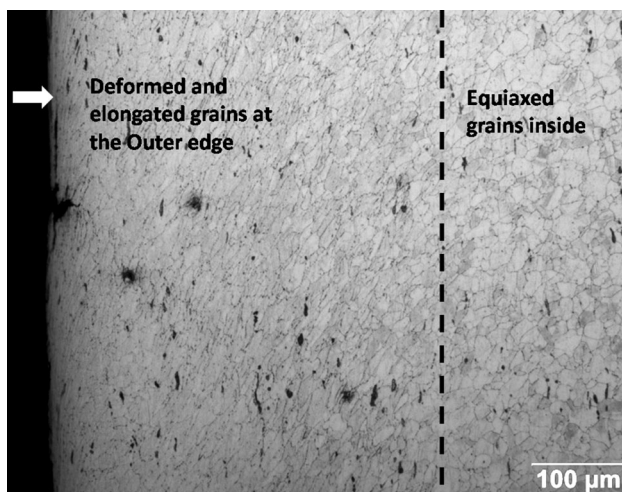


Fig. 14 Optical micrographs showing deformed and elongated grains at the outer diameter up to approximately 400 μm inside and equiaxed grains at interior of the sleeve

microscopic observations (Fig. 13c) at the OD side suggest that they were generated on the surface during the swaging operation. The reasons for formation of micro-cracks on the surface are attributed to the combined effect of large plastic strain developed on the OD surface of the sleeve and

sensitized microstructure of the material. The plastic strain on the surface will be more, if the die used for swaging operation has a rough surface. The rough surface along with longitudinal die marks on the sleeve indicates that the dies used for swaging operation had a poor surface finish which introduced large plastic strain on the surface of the sleeve.

The plastic strain on the sleeve is indicated by deformed and elongated grain at outer edge as shown in Fig. 14. The larger plastic strain and small size micro-cracks formed on the OD surface of the sleeve can be seen in Fig. 13c. Larger plastic strain at the OD surface has also resulted in higher hardness to a magnitude of 470 $\text{HV}_{100\text{gf}}$. The Vickers hardness of AISI 304 steel tends to increase proportionally with increases in cold working as reported by Singh et al. [1]. This indicates that the OD surface of the sleeve has undergone extensive cold reduction on the surface, whereas the extent of cold reduction decreased towards—the interior surface as shown in Fig. 14. This is reflected as variation in grain elongation and flow from the OD surface to the inside of the sleeve. Microscopic observations indicated that deformed and elongated grains were present up to 400 μm . This results in the generation of residual stresses due to the gradient in the plastic strain along the thickness direction.

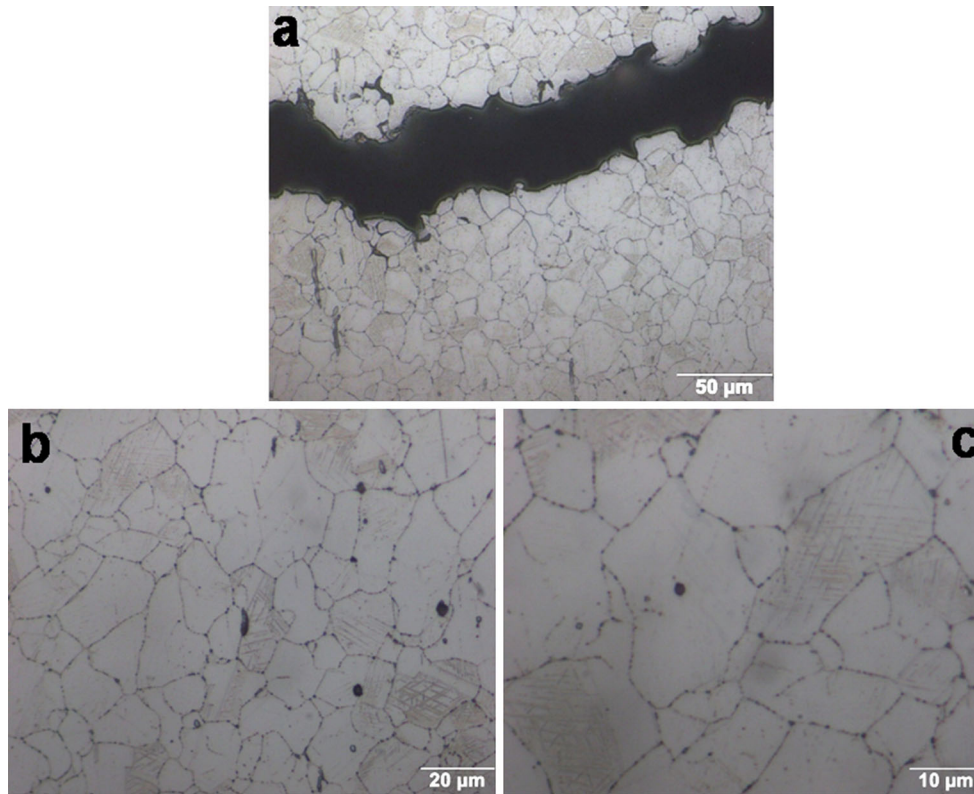
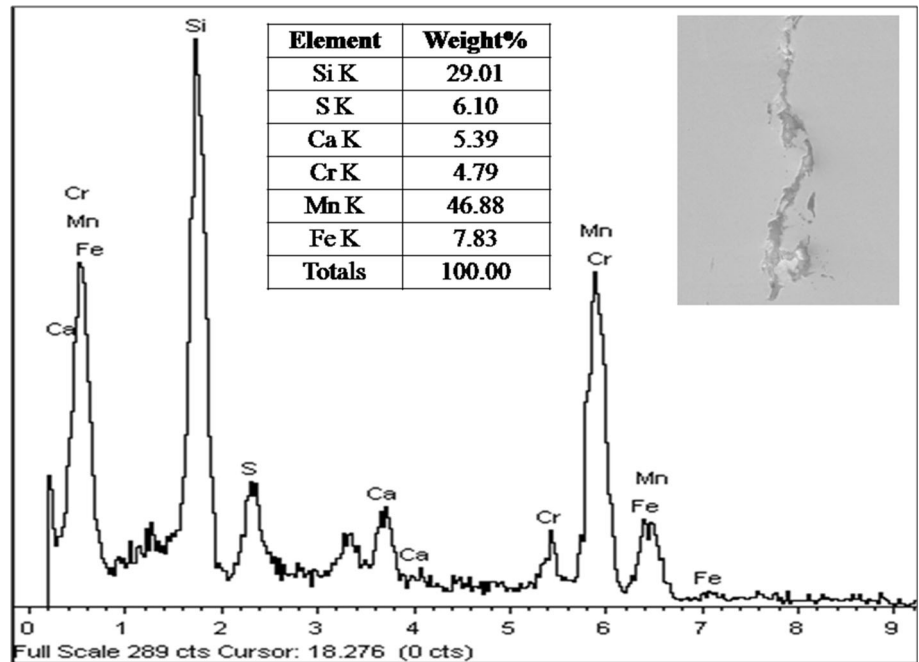


Fig. 15 Optical micrographs showing (a) cracking along the grain boundaries, (b, c) chromium carbide precipitation at the grain boundaries

Fig. 16 EDS spectrum showing chemical composition of silicate inclusion



Singh et al. [1] reported that for 80% cold rolling, the hardness was 466 HV_{100gf}; this indicates that the plastic strain on the outer surface of sleeve has crossed 80%

reduction. It was also reported that deformation induced martensite forms with the cold deformation of this steel [1–3]. It was reported that at 80% cold reduction, the

Fig. 17 EDS spectrum showing chemical composition of sulphide inclusion

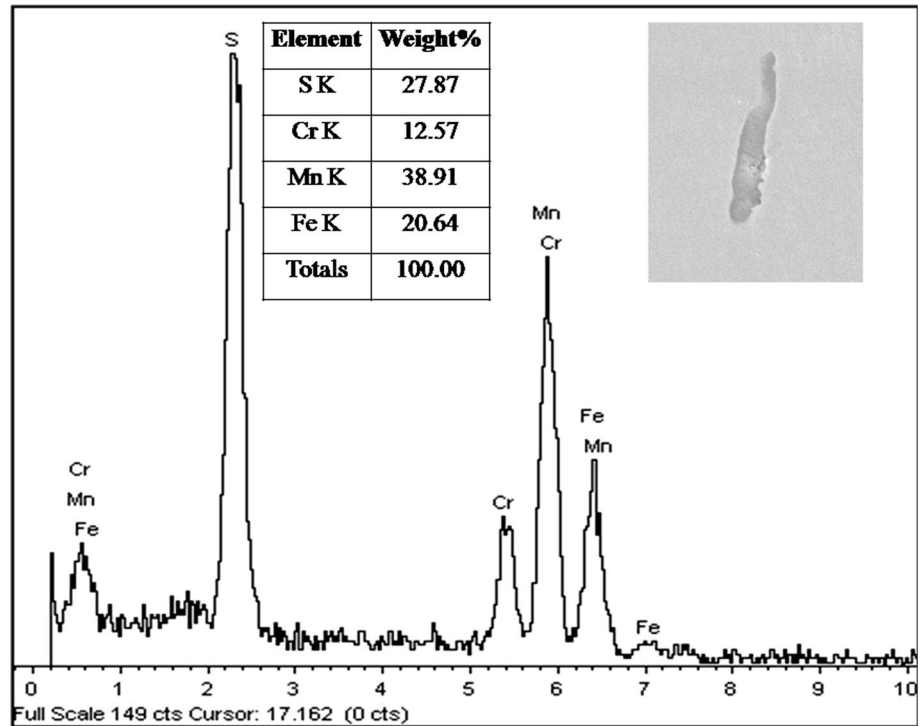
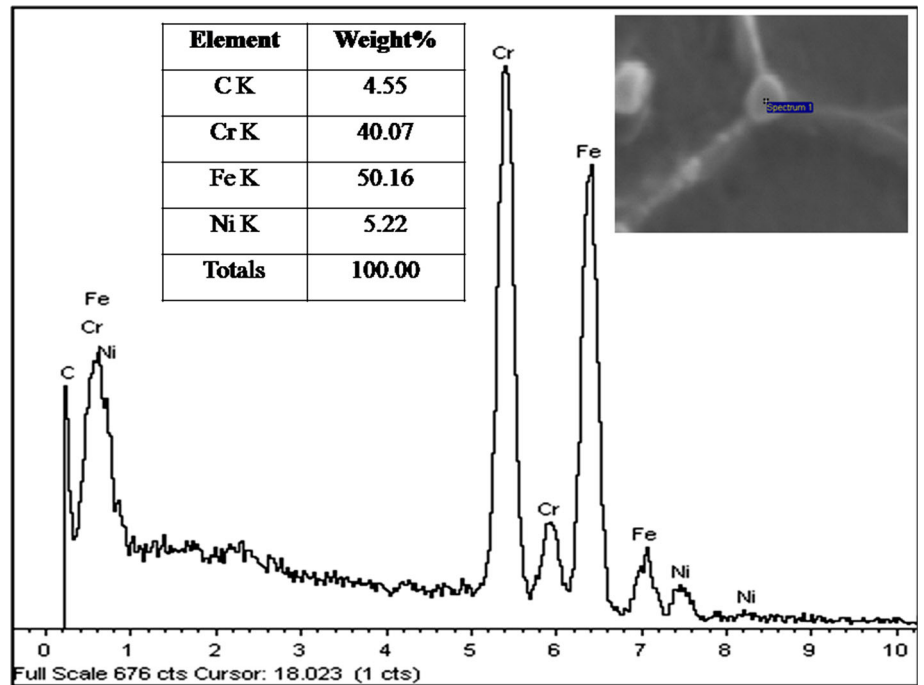


Fig. 18 EDS spectrum showing chemical composition of chromium carbide precipitation at grain boundaries



martensite is a dominant phase in AISI 304 stainless steel. The formation of deformation induced martensite was also collaborated with increase in hardness of cold-worked steels [1].

The residual stresses present in the component along with the stresses due to swaging operation are responsible for subsequent growth of micro-cracks under a no-stress condition. The observation of the primary circumferential

crack near to centre of the sleeve is due to the large stresses at that location. It was also noticed that additional cracks on either side of primary crack have grown up to 250 and 400 μm size. The primary circumferential crack encountered the long silicate inclusions aligned in a longitudinal direction during the crack propagation leading to deviation in the crack path along the longitudinal direction. The microstructure exhibits uniformly distributed oxide and manganese sulphide inclusions and isolated long silicate stringers. Fractographic observations (Fig. 7) indicated debonding at the inclusion–matrix interface of these manganese sulphide inclusions during crack propagation.

Sulphur is soluble in molten steel, but its solubility in solid steel is very low and hence it is precipitated in the form of sulphides during the solidification of the steel and its precipitation pattern is influenced by its strong segregation tendency [4]. During solidification, the interdendritic liquid gets enriched in the solute content and liquid oxysulphide starts to form. During cooling, iron–manganese oxysulphide remains liquid until the temperature decreases and if sufficient oxygen and sulphur are present in the steel, liquid oxysulphide phase is present at temperature above 900 $^{\circ}\text{C}$ depending on manganese content in steel. In steels, the sulphur will be in the form of MnS due to the high solubility product of sulphide and oxysulphide of manganese in liquid iron. It forms only in solute-enriched interdendritic liquid during solidification of steel [5]. MnS inclusions get deformed and oriented in the direction of thermo-mechanical processing forming stringers. The elongated MnS stringers present in the steel affect the mechanical properties, notch toughness and ductility [6, 7].

Most silicate inclusions have several oxide components, for example MnO, FeO, CaO, Al_2O_3 and SiO_2 . Silicate inclusions have a low index of deformability at lower temperatures and thus are brittle during cold working of the steel [4]. The presence of isolated long silicate stringers up to 2.2 mm size in the sleeve material was more detrimental

because they provide a very long and continuous weak interface for crack propagation. Isolated long silicate stringers were responsible for the identified deviation of the primary crack and subsequent crack propagation leading to fast fracture. The cracks have propagated in an intergranular manner due to the hard and brittle continuous chromium carbide precipitation along the grain boundaries and residual stresses present in the component along with assembly stresses.

The chromium carbide precipitation along the grain boundary is called the sensitization of the steel. Sensitization is one of the embrittlement (loss of ductility) phenomena in austenitic stainless steels. In austenitic stainless steels, chromium carbides dissolve completely in the matrix at approximately above 1035 $^{\circ}\text{C}$. When the steels cooled slowly from these higher temperatures or reheated to the temperature range of 425–815 $^{\circ}\text{C}$, chromium carbides are precipitated along the grain boundaries. During annealing of austenitic stainless steel, it is cooled rapidly by water quenching to prevent the sensitization. The rate of carbide precipitation varies significantly with the carbon content in the steel. AISI 304 steel containing 0.05% carbon can be free of sensitization under the cooling conditions which produced heavy sensitization in the same alloy with 0.08% carbon [8]. Hence to avoid the problem of sensitization, extra-low-carbon stainless steel AISI 304L is commonly used. AISI 304L grade steel has carbon content of 0.03% compared to 0.08% carbon present in normal AISI 304 steel [9, 10].

Based on the above observations and discussion, the failure of AISI 304 steel sleeve was due to the large plastic strain, the presence of residual stresses along with assembly stresses and embrittlement caused by sensitized microstructure. The continuous grain boundary network of chromium carbide precipitation led to cracking of sleeve by brittle intergranular mode. The presence of silicate inclusion stringers was responsible for easy crack propagation and deviation of the primary crack.

Table 1 Details of the qualification tests carried out for acceptance of the hose assembly for flight use

Sl. no.	Qualification tests	Remarks
1.	Dye penetration test on swaged area	To detect surface cracks on swaged surface
2.	Pneumatic pressure test	For joint leak tightness under pneumatic pressure of 1 MPa
3.	Working pressure and proof pressure test	Verifying integrity and leak tightness at 22 and 33 MPa
4.	High temperature test followed by proof pressure test	Soak at 260 $^{\circ}\text{C}$ for 3 h
5.	Low temperature test followed by proof pressure test	Soak at -45 $^{\circ}\text{C}$ for 3 h
6.	Pressure hold test for 24 h	At operating pressure 22 MPa
7.	Impulse pressure test	Verification for fatigue failures cycling at the rate of 9 cycles/20 s for 5000 cycle between 0 and 33 MPa
8.	Burst pressure test	At 44 MPa pressure
9.	Pneumatic pressure test (Post)	For joint leak tightness under pneumatic pressure of 1 MPa
10.	Vibration test at assembly level	Verification for fatigue failures

Subsequent to the failure, the material of the sleeve was changed from SS304 to SS304L grade material conforming to material acceptance criterion with respect to inclusion rating, microstructure and mechanical properties.

The SS304L grade steel was selected to avoid the problem of chromium carbide precipitation at grain boundaries. The swaging procedure was modified to minimize the strain at the failed location of the sleeve of the hose assembly, and the surface quality of dies was ensured. With the change in material grade and modified procedure, subsequent hose assemblies have passed all of the stipulated qualification tests listed in Table 1.

Conclusion

The crack in the sleeve initiated from the OD surface and propagated inwards in an intergranular mode. The intergranular brittle mode of failure was attributed to the large plastic strain, the presence of residual, assembly stresses and embrittlement caused by the sensitized microstructure. The sensitized microstructure having a continuous grain boundary network of chromium carbide precipitation promoted crack propagation in a brittle intergranular manner. The silicate inclusion stringers were responsible for enhanced crack propagation with some deviation of the primary crack.

It was recommended that the sleeve material be changed from AISI 304 to AISI 304L grade stainless steel with controlled inclusions to avoid the problem of chromium carbide precipitation at grain boundaries and inclusion stringers. Modification of the swaging process was

suggested for minimizing the plastic strain at the failure location and reducing the induced residual stresses.

Acknowledgments Authors wish to thank Director, VSSC for the continuous support in carrying out the study and for permitting to publish the paper.

References

1. R. Singh, B. Ravikumar, A. Kumar, P.K. Dey, I. Chattoraj, The effects of cold working on sensitization and intergranular corrosion behavior of AISI 304 stainless steel. *Metall. Mater. Trans. A* **34A**, 2441–2447 (2003)
2. A. Das, S. Sivaprasad, M. Ghosh, P.C. Chakraborti, S. Tarafder, Morphologies and characteristics of deformation induced martensite during tensile deformation of 304 LN stainless steel. *Mater. Sci. Eng. A* **486**, 283–286 (2008)
3. V. Kain, K. Chandra, K.N. Adhe, P.K. De, Effect of cold work on low temperature sensitization behavior of austenitic stainless steels. *J. Nucl. Mater.* **334**, 115–132 (2004)
4. R. Kiessling, *Non-metallic inclusions in steel*, 2nd edn. (The Metals Society, London, 1977)
5. E.T. Turkdogan, Theoretical aspects of sulphide formation in steel, in *Sulphide inclusions in steel* (ASM, 1975), pp. 1–22
6. I. Kozasu, J. Tanaka, Effects of sulphide inclusions on notch toughness and ductility of structural steels, in *Sulphide inclusions in steel* (ASM, 1975), pp. 286–308
7. A.J. DeArdo, Jr., E.G. Hamburg, Influence of elongated inclusions on the mechanical properties of high strength steel plate, in *Sulphide inclusions in steel* (ASM, 1975), pp. 309–337
8. J.R. Davis, *Metals Handbook* (Materials Park, ASM International, 1998). **Desk edition**
9. Aerospace Material Specification, AMS-5647H, SAE Aerospace (2007)
10. Aerospace Material Specification, AMS-5639H, SAE Aerospace (2007)